1 **Quantification of environmentally persistent free radicals and reactive**

2 **oxygen species in atmospheric aerosol particles**

3

4 Andrea M. Arangio[1], Haijie Tong[1], Joanna Socorro[1], Ulrich Pöschl[1] & Manabu Shiraiwa[1],*

5 [1] Multiphase Chemistry Department, Max Planck Institute for Chemistry, Mainz, Germany

6 * m.shiraiwa@mpic.de

7

8

9

10 **Abstract**

11 Fine particulate matter plays a central role in adverse health effects of air pollution.

12 Inhalation and deposition of aerosol particles in the respiratory tract can lead to the release of

13 reactive oxygen species (ROS), which may cause oxidative stress. In this study, we have

14 detected and quantified a wide range of particle-associated radicals using electron

15 paramagnetic resonance (EPR) spectroscopy. Ambient particle samples were collected using

16 a cascade impactor at a semi-urban site in central Europe, Mainz, Germany in May – June

17 2015. Concentrations of environmentally persistent free radicals (EPFR), most likely

18 semiquinone radicals, were found to be in the range of $(1 - 7) \times 10^{11}$ spins μg^{-1} for particles in

19 the accumulation mode, whereas coarse particles with a diameter larger than 1 μm did not

20 contain substantial amounts of EPFR. Using a spin trapping technique followed by

21 deconvolution of EPR spectra, we have also characterized and quantified ROS including OH,

22 superoxide (O_2^-) and carbon- and oxygen-centred organic radicals, which were released upon

23 extraction of the particle samples in water. Total ROS amounts of $(0.1 - 3) \times 10^{11}$ spins μg^{-1}

24 were released by submicron particle samples and the relative contributions of OH, O_2^-, C-

25 centred and O-centred organic radicals were ~11 - 31%, ~2 – 8%, ~41 – 72% and ~0- 25%,

26 respectively, depending on particle sizes. OH was the dominant species for coarse particles.

27 Based on comparisons of the EPR spectra of ambient particulate matter with those of

28 mixtures of organic hydroperoxides, quinones and iron ions followed by chemical analysis

29 using liquid chromatography mass spectrometry (LC-MS), we suggest that the particle-

30 associated ROS were formed by decomposition of organic hydroperoxides interacting with

31 transition metal ions and quinones contained in atmospheric humic-like substances (HULIS).

32

Atmospheric
Chemistry
and Physics
Open Access
EGU
Discussions

1. Introduction

Epidemiological studies have clearly shown positive correlations between respiratory diseases and ambient fine particulate matter (Pope and Dockery, 2006; Strak et al., 2012; West et al., 2016). A recent study has estimated that outdoor air pollution leads to 3.3 million premature deaths per year worldwide, which is mostly due to particular matter with a particle diameter less than 2.5 μm ($PM_{2.5}$) (Lelieveld et al., 2015). Plausible reasons include the cytotoxicity of ambient $PM_{2.5}$ and its ability to induce inflammatory responses by oxidative stress causing functional alterations of pulmonary epithelial cells (Nel, 2005; Gualtieri et al., 2009). Oxidative stress is mediated by reactive oxygen species (ROS) including OH, H_2O_2, superoxide (O_2^-), as well as organic radicals (Winterbourn, 2008; Pöschl and Shiraiwa, 2015). Upon PM deposition into the respiratory tract and interactions with lung antioxidants, H_2O_2 can be generated by redox-active components contained in $PM_{2.5}$ such as transition metals (Charrier et al., 2014; Fang et al., 2015), semiquinones (Kumagai et al., 1997; Cho et al., 2005; Khachatryan et al., 2011; McWhinney et al., 2013), and humic-like substances (Kumagai et al., 1997; Cho et al., 2005; Lin and Yu, 2011; Charrier et al., 2014; Dou et al., 2015; Fang et al., 2015; Verma et al., 2015b). H_2O_2 can be converted into highly-reactive OH radicals via Fenton-like reactions with iron and copper ions (Charrier et al., 2014; Enami et al., 2014).

Ambient particles have been found to contain large amounts of ROS (mostly H_2O_2) in the particle phase (Hung and Wang, 2001; Venkatachari et al., 2005; Venkatachari et al., 2007; Fuller et al., 2014). Substantial amounts of particle-bound ROS are found on biogenic secondary organic aerosols (SOA) produced from the oxidation of α-pinene, linalool, and limonene (Chen and Hopke, 2010; Chen et al., 2011; Pavlovic and Hopke, 2011; Wang et al., 2011; Wang et al., 2012). Recently, Tong et al. (2016) have shown that terpene and isoprene SOA can form OH radicals upon interactions with liquid water and iron ions under dark conditions. This can be explained by the decomposition of organic hydroperoxides, which account for the predominant fraction of SOA mass and are generated via multigenerational oxidation and autoxidation (Docherty et al., 2005; Ziemann and Atkinson, 2012; Crounse et al., 2013; Ehn et al., 2014; Epstein et al., 2014; Badali et al., 2015).

In addition, $PM_{2.5}$ contain environmentally persistent free radicals (EPFR) that can be detected directly by electron paramagnetic resonance (EPR) spectroscopy (Dellinger et al., 2001; Khachatryan et al., 2011; Gehling and Dellinger, 2013). EPFR are stable radicals with an e-folding lifetime exceeding one day (Gehling and Dellinger, 2013; Jia et al., 2016). The chemical nature of EPFR is remarkably similar to semiquinone radicals, which can be

67 stabilized via electron transfer with transition metals in the particle phase (Truong et al., 2010;

68 Vejerano et al., 2011; Gehling and Dellinger, 2013). EPFR are formed upon combustion and

69 pyrolysis of organic matter (Dellinger et al., 2001; Dellinger et al., 2007). The formation of

70 stable radicals can also be induced by heterogeneous and multiphase chemistry of organic

71 aerosols. Heterogeneous ozonolysis of aerosol particles such as polycyclic aromatic

72 hydrocarbons (PAH) and pollen proteins can lead to the formation of long-lived reactive

73 oxygen intermediates (ROI) (Shiraiwa et al., 2011; Shiraiwa et al., 2012; Reinmuth-Selzle et

74 al., 2014; Borrowman et al., 2015; Kampf et al., 2015; Berkemeier et al., 2016).

75   In this work, ambient particles with a diameter in the range of 56 nm to 3.2 μm were

76 collected using a cascade impactor during May – July 2015 in Mainz, Germany. Size

77 dependences of EPFR concentrations contained in ambient particles have been measured

78 using an EPR spectrometer. Particles were also extracted in water containing a spin-trapping

79 agent followed by EPR analysis to quantify the formation of various radical forms of ROS

80 including OH, superoxide (O_2^-) and carbon- and oxygen-centred organic radicals.

81

82 **2. Methods**

83   Ambient particles were collected using a micro-orifice uniform deposition impactor

84 (MOUDI, 110-R mode, MSP Corporation) on the roof of the Max Planck Institute for

85 Chemistry, Mainz, Germany (49.99 N, 8.23 E). The sampling was conducted every 24 h

86 starting at 5 PM during 28 May - 9 June 2015. Particles were collected with a sampling time

87 of 48 h during 26-27 June and 18-19 July 2015. The sampling was conducted with a flow rate

88 of 30 L min^{-1} with the following nominal lower cut-off particle diameters: 56, 100, 180, 320,

89 560 nm, 1 μm, and 1.8 μm. Particles were collected on 47 mm diameter Teflon filters (100

90 nm pore size, Merck Chemicals GmbH). Each filter was cleaned and sonicated for 10 min

91 with pure ethanol and ultra-pure water and dried with nitrogen gas before weighing. Teflon

92 filters were weighed four times using a balance (Mettler Toledo XSE105DU). Particles were

93 extracted by immersing the filter into a solution containing 350 μL of 20 mM 5-tert-

94 Butoxycarbonyl-5-methyl-1-pyrroline-N-oxide (BMPO, high purity, Enzo Life Sciences

95 GmbH) and stirred with a vortex shaker (Heidolph Reax 1) for 7-9 min. BMPO is an efficient

96 spin-trapping agent for OH, O_2^- and organic radicals (Zhao et al., 2001; Tong et al., 2016).

97 Extracts were dried for approximately 14-17 min under 1-3 bar N_2 flow and the final volume

98 of the sample for EPR measurements was 50 μL.

99   A continuous-wave electron paramagnetic resonance (CW-EPR) X-band spectrometer

100 (EMXplus-10/12, Bruker, Germany) was used for detection and quantification of stable

Atmospheric
Chemistry
and Physics
Discussions

Open Access

EGU

101   radicals and ROS. Filters containing particles were folded and introduced into a 4 mm i.d.

102   quartz tube and inserted directly into a high sensitivity cavity. EPR spectra were recorded at a

103   room temperature of 23 °C by setting the following operating parameters: a modulation

104   frequency of 100 kHz; a microwave frequency of 9.84 GHz; a microwave power of 2.149

105   mW (20 db); a modulation amplitude of 1.0 G; a sweep width of 110.0 G; a sweep time of

106   175 s; a receiver gain of 40 db; a time constant of 40.96 ms; a conversion time of 160 ms; and

107   a scan number of 6. The spin-counting method embedded in the Bruker software Xenon was

108   used to quantify detected radicals. The spin-counting method was calibrated using a standard

109   compound 4-hydroxy-2,2,6,6-tetramethylpiperidin-1-oxyl (TEMPOL). The detection limit of

110   EPR was ~1×10^{10} spins per µg of particle mass in this study. For better quantification and

111   determination of the relative contributions of OH, O_2^-, carbon-centred and oxygen-centred

112   organic radicals, EPR spectra were fitted and simulated using Xenon and the Matlab-based

113   computational package Easyspin (Stoll and Schweiger, 2006).

114

115   **3. Results and discussion**

116   **3.1. Environmentally persistent free radicals**

117   Figure 1 shows EPR spectra of ambient particles in the lower cut-off diameter range of

118   56 nm – 1.8 µm. Fine particles, with lower cut-off diameters of 56 - 320 nm, show a single

119   and unstructured peak with a g-factor of ~2.003 and with a peak to peak distance (ΔH_{p-p})

120   ranging from 3 to 8 G. Such spectra are characteristic for EPFR, which have been attributed

121   to semiquinone radicals (Dellinger et al., 2001; Dellinger et al., 2007; Vejerano et al., 2011;

122   Bahrle et al., 2015). Particles with a diameter smaller than 56 nm and larger than 560 nm did

123   not show significant signals, indicating the reduced amount of EPFR in these size ranges.

124   EPR spectra for particles with the lower cut-off diameters of 56 – 320 nm for each sampling

125   day are presented in Fig. A1.

126   The black line in Fig. 2 shows the size distribution of EPFR concentrations. Particles

127   with different sizes had different radical contents and particles with the lower cut-off

128   diameter of 100 nm contained the highest EPFR concentrations of $7.0(\pm0.7) \times 10^{11}$ spins µg^{-1}.

129   High abundances of EPFR in particles in the accumulation mode is consistent with mass size

130   distributions of combustion-generated particles such as soot or black carbon, which typically

131   have peak concentrations around 100 – 200 nm (Bond et al., 2013).

132   Figure 3 shows the temporal evolution of EPFR concentrations contained in particles

133   with lower cut-off diameters of 100 and 180 nm. During the sampling period of two weeks,

134   there were two rain events (on 30 May 2015 and 1 June 2015) and three sunny days (4-6 June

Atmospheric
Chemistry
and Physics
Discussions

Open Access

EGU

135 2015), and the other days were cloudy. The mass concentrations of particles within the

136 diameters of 56 - 560 nm were in the range of 3.9 – 12.8 µg m^{-3}. Maximum values of ~7 ×

137 10^{11} spins µg^{-1} were reached during sunny days, indicating that photochemistry may be

138 related to EPFR production. For example, heterogeneous reactions of photo-oxidants

139 including O_3 and OH with soot or PAH may contribute to the formation of long-lived radicals

140 (Shiraiwa et al., 2011; Borrowman et al., 2015). Radical concentrations were as low as 6.3 ×

141 10^{10} spins µg^{-1} during rain events, most likely due to low production of EPFR and scavenging

142 by precipitation.

143 EPFR concentrations contained in particles collected for 48 h during 26-27 June 2015

144 was ~2.2 × 10^{11} spins µg^{-1}. EPFR concentrations contained in particles within the diameter of

145 56 – 560 nm averaged over the entire measurement period was 2.0(±1.3) × 10^{11} spins µg^{-1}.

146 Squadrito et al. (2001) determined the EPFR concentrations to be in the range of (1-10) ×10^{11}

147 spins µg^{-1} in $PM_{2.5}$ sampled for 24 h in five different urban sites in the United States. Gehling

148 et al. (2014) reported that the EPFR concentration was in the range of (7-55)×10^{10} spins µg^{-1}

149 at a site in Louisiana near heavy interstate traffic along a major industrial corridor of the

150 Mississippi River. Shaltout et al. (2015) measured radical concentrations in the range of (2-6)

151 ×10^{10} spins µg^{-1} in $PM_{2.5}$ collected in industrial-, residential- and traffic-dominated sites in

152 Taif city, Saudi Arabia. These values are comparable with the EPFR concentrations measured

153 in this work.

154

155 **3.2. Reactive oxygen species**

156 Figure 4a shows EPR spectra of ambient particles with lower cut-off diameters of 56

157 nm - 1.8 µm extracted in water with the spin-trapping agent BMPO. Each EPR spectrum is

158 composed of several overlapped lines, originating from different radical forms of ROS.

159 Dashed lines indicate the positions of each peak for each type of trapped ROS including OH

160 (green), superoxide (red), carbon-centred (orange) and oxygen-centred organic radicals (blue).

161 The relative abundance of these radicals was different for each size range, causing the EPR

162 spectral features to be highly variable. For example, spectra from particles larger than 1.0 µm

163 consist mainly of four peaks that are typical for OH radicals, whereas those for smaller

164 particles contain more peaks indicating the presence of multiple radicals.

165 To estimate the relative amount of each type of ROS, the observed EPR spectra were

166 fitted and simulated using the software Easyspin 5.0 and Xenon. Four types of radicals have

167 been used to fit the spectra: BMPO-OH (hyperfine coupling constants of $a^N = 14.3$ G, $a^H_\beta =$

168 12.7 G, $a^H_\gamma = 0.61$ G), BMPO-OOH ($a^N = 14.3$ G, $a^H = 8.1$ G), BMPO-R ($a^N = 15.2$ G, $a^H =$

169   21.6 G) and BMPO-OR (a^N = 14.5 G, a^H_β = 16.6 G). As shown in Fig. 4b, the simulated EPR

170   spectrum reproduced the observed spectrum very well with a small residual. The

171   deconvolution of spectra allowed us to estimate the relative contribution of four types of ROS

172   within each particle size range.

173   Figure 5 shows the relative contributions of OH (green), superoxide (red), carbon-

174   centred (orange) and oxygen-centred (blue) organic radicals to the total radicals trapped by

175   BMPO in each particle size range. Carbon-centred radicals are the most abundant type of

176   radicals, contributing ~50 - 72% of total ROS for PM1. It decreases to 41% and 9% for

177   particles with lower cut-off diameters of 1 μm and 1.8 μm, respectively. The OH radical

178   accounts for ~11 – 31% of total trapped radicals for PM1, whereas OH was the dominant

179   species for coarse particles with diameters of 1.8 – 3.2 μm. The least abundant radical for all

180   size ranges was O_2^-, with contributions of ~2 - 8% and without any clear size dependence.

181   The amount of oxygen-centred organic radicals ranges between 12% and 25% in particles

182   with a diameter below 1 μm and its contribution was negligible for coarse particles. Note that

183   the contribution of oxygen-centred organic radicals for particles with a diameter of 1 – 1.8

184   μm might be attributed to the OH radical: the hyperfine coupling constants for BMPO-OR for

185   better fitting the spectrum for this size range needed to be changed slightly (a^N = 13.5 G, a^H_β

186   = 15.3 G, a^H_γ = 0.6 G). These values are similar to constants of a second conformer of

187   BMPO-OH.

188   The red line in Fig. 2 shows the size-dependent concentrations of radical forms of ROS

189   (e.g., sum of OH, O_2^-, C- and O- centred organic radicals). Particles with the lower cut-off

190   diameter of 100 nm have the highest ROS concentrations of 2.7(±0.2) × 10^{11} spins μg^{-1}.

191   Concentrations are smaller for particles in the coarse mode with a diameter larger than 1 μm.

192   This is consistent with previous studies, suggesting that particles in the accumulation mode

193   are the most active in ROS generation (Hung and Wang, 2001; Venkatachari et al., 2007;

194   Saffari et al., 2013; Wang et al., 2013; Saffari et al., 2014). The total concentration of radical

195   forms of ROS was measured to be 1.2 × 10^{11} spins μg^{-1}. Note that O_2^- concentrations might

196   be underestimated as the lifetime of the BMPO-OOH adduct is relatively short (~20 min)

197   (Ouari et al., 2011; Abbas et al., 2014).

198   Previous studies have measured redox activity and oxidative potential of PM by the

199   dichlorofluorescein (DCFH) and dithiothreitol (DTT) assays. The DCFH assay is mostly

200   sensitive to H_2O_2 and other peroxides. For example, Hung and Wang (2001) reported ROS

201   concentrations as 1×10^{13} μg^{-1} in Taipei, Taiwan. This value is very similar to H_2O_2

202   concentrations contained in ambient PM$_{2.5}$, which has been quantified to be up to 1×10^{13} μg^{-1}

Atmospheric
Chemistry
and Physics
Discussions

Open Access

203 in an urban environment in southern California using HPLC fluorescence (Wang et al., 2012).

204 The DTT assay is based on the decay of DTT due to redox reactions with PM components,

205 reporting the oxidative potential of PM in moles of DTT consumed per unit of time and mass

206 of PM. Verma et al. (2015a) and Fang et al. (2015) reported that $PM_{2.5}$ sampled in an urban

207 environment in Atlanta, Georgia, USA has a DTT activity in the range of 10-70 pmol min^{-1}

208 μg^{-1}. Assuming an integration time of 20 min needed for the extraction of PM in this work,

209 this value corresponds to $(1-8)\times10^{14}$ μg^{-1} of DTT molecules consumed. Charrier et al. (2012)

210 also reported that $PM_{2.5}$ sampled in an urban environment in Fresno, California USA has a

211 DTT activity of 27 - 61 pmol $min^{-1}\mu g^{-1}$, corresponding to $(2 – 7)\times10^{14}$ μg^{-1} of DTT molecules

212 consumed in 20 min. These comparisons imply that the total ROS associated with ambient

213 particles are likely to be dominated by H_2O_2, which is about a few orders of magnitude more

214 abundant than radical forms of ROS determined by EPR in this study. This is reasonable as

215 H_2O_2 is closed shell and much more stable than open-shell radical ROS species.

216

217 3.3. ROS formation mechanism

218 It has been shown that semiquinones and reduced transition metals including Fe(II) and

219 Cu(I) can react with O_2 to form O_2^-, which can be further converted to H_2O_2 (Gehling et al.,

220 2014; Fang et al., 2015). Fenton-like reactions of H_2O_2 with Fe(II) or Cu(I) can lead to the

221 formation of OH radicals (Winterbourn, 2008; Pöschl and Shiraiwa, 2015). OH radicals can

222 also be generated by the decomposition of organic hydroperoxides (ROOH) contained in

223 SOA, yielding RO radicals (Tong et al., 2016). Several studies have reported a metal-

224 independent decomposition of hydroperoxides and organic hydroperoxides driven by

225 substituted quinones producing RO radicals (Sanchez-Cruz et al., 2014; Huang et al., 2015).

226 The presence of Fe(II) or quinones is suggested to enhance ROOH decomposition and the

227 formation of RO and OH radicals (Zhu et al., 2007a; Zhu et al., 2007b; Zhu et al., 2009;

228 Sanchez-Cruz et al., 2014). Organic peroxides (ROOR) do not yield OH and RO radicals

229 even in the presence of iron ions (Tong et al., 2016).

230 Based on these previous studies and considering that ambient particles may contain

231 quinones, organic hydroperoxides, and transition metals, the observed ROS formation may be

232 caused by interactions of these chemical components. To further investigate this aspect,

233 mixtures of organic hydroperoxides, quinones, and Fe(II) were analysed by EPR and liquid

234 chromatography mass spectrometry (LC-MS). Two standard organic hydroperoxides, cumene

235 hydroperoxide and tert-butyl hydroperoxide, were used. For quinones, p-benzoquinone and

Atmospheric
Chemistry
and Physics
Discussions

236   humic-like substances are used, as HULIS are known to contain substantial amounts of

237   quinones.

238   Figure 6 shows the comparison of EPR spectra of ambient particles with a diameter of

239   180 - 320 nm (black) sampled on 26 June 2015 (same as shown in Fig. 4) and the above

240   mixtures of organic compounds. Panel (a) includes EPR spectra of mixtures of all three

241   different components (ROOH, quinone, metal) and panel (b) presents mixtures of two

242   different components. All three of the organic mixtures in panel (a) resemble the EPR

243   spectrum of ambient particles by reproducing almost all of the peaks. Particularly, the EPR

244   spectrum of the mixture containing cumene hydroperoxide, humic acid and Fe(II) closely

245   overlaps with the ambient particle EPR spectrum. Similarity of spectra between p-

246   benzoquinone and HULIS suggests that the chemical nature of quinones and HULIS is very

247   similar. Note that peaks related to the BMPO-OOH adduct at 3497 G and at 3530 G are more

248   prominent in standard organic mixtures compared to ambient particles. This may be due to

249   the relatively short lifetime of BMPO-OOH of ~23 min (Zhao et al., 2001), which is

250   comparable to the extraction and mixing time of BMPO with the atmospheric particles (21 –

251   28 min), during which BMPO-OOH may have decayed. The trapped radicals have been

252   further characterized by LC-MS, confirming the presence of OH and semiquinone radicals as

253   well as carbon- and oxygen centred organic radicals, as detailed in Appendix A and Figs. A1

254   and A2.

255   EPR spectra of mixtures containing two compounds in panel (b) reproduce only a part

256   of the observed peaks. These observations strongly suggest that the combination of these

257   three chemical components play an important role in generating ROS species by atmospheric

258   particles. The role of transition metals is crucial to enhance radical formation, most likely via

259   Fenton-like reactions (Tong et al., 2016) and by participating in redox-cycling of quinones

260   (Khachatryan and Dellinger, 2011), as intensities of EPR spectra without Fe(II) (CHP +

261   HULIS, dark blue; CHP + pBq, orange) are small. Carbon-centred radicals may have

262   multiple sources such as the decomposition of the BMPO-OR adduct by scission of the

263   carbon in β position, yielding for example CH_3 radicals (Zhu et al., 2007b; Huang et al., 2015)

264   as detected by LC-MS (Fig. A2). They may also be generated by secondary reactions of non-

265   trapped OH radicals with water-soluble organic compounds.

266   SOA particles, which may contain large amounts of organic hydroperoxides, account

267   for a major fraction in PM1 (Jimenez et al., 2009). SOA compounds may also coat coarse

268   particles such as biological particles (Pöhlker et al., 2012). As shown in Fig. 2, semiquinones

269   are mostly contained in submicron particles but not in coarse particles. Thus, the release of a

Atmospheric
Chemistry
and Physics
Discussions

270 variety of ROS species are most likely due to the interactions of organic hydroperoxides,

271 semiquinones, and transition metal ions, whereas the dominance of OH radicals in coarse

272 particles may be due to the decomposition of organic hydroperoxides in the absence of

273 semiquinones.

274

275 **4. Conclusions and implications**

276 In this study particle-associated environmentally persistent free radicals (EPFR) and

277 radical forms of ROS have been quantified using electron paramaganetic resonance (EPR)

278 spectroscopy. EPFR concentrations were measured to be ~2×10^{11} spins μg^{-1}. The chemical

279 identity of EPFR is likely to be semiquinone radicals based on the g-factors observed by EPR

280 spectroscopy. We found that particles with different sizes had different radical contents and

281 particles with a diameter of 100 - 180 nm had the highest abundance of EPFR, whereas

282 coarse particles did not contain EPFR. This is consistent with the size distribution of

283 combustion particles such as soot and humic-like substances (HULIS), which may contain

284 substantial amounts of EPFR.

285 Reactive oxygen species (ROS) are realeased upon extraction of particles into water.

286 Particles with the diameter of 100 – 180 nm have released the highest ROS concentrations of

287 $2.7(\pm 0.2) \times 10^{11}$ spins μg^{-1}. By deconvoluting the obtained EPR spectra, four types of radicals,

288 including OH, O_2^-, carbon-centred and oxygen-centred organic radicals were quantified. The

289 relative amounts of OH, O_2^-, C-centred and O-centred organic radicals in submicron particles

290 were found to be ~11 - 31%, ~2 – 8%, ~41 – 72% and ~0- 25%, respectively, depending on

291 the particle size. OH was the dominant species for coarse particles with a diameter larger than

292 1 μm. We suggest that the formation of these ROS species is due to the decomposition of

293 organic hydroperoxides, which are a major component in SOA, interacting with

294 semiquinones contained in soot or HULIS. ROS formation can be enhanced in the presence

295 of iron ions by Fenton-like reactions.

296 These findings have significant implications for the chemical processing of organic

297 aerosols in deliquesced particles and cloud water. The released OH radicals within particles

298 or cloud droplets can oxidize other organic compounds, producing low-volatility products

299 including organic acids, peroxides, and oligomers (Lim et al., 2010; McNeill et al., 2012;

300 Ervens, 2015; Herrmann et al., 2015). Autoxidation in the condensed phase might be

301 triggered by OH radicals forming highly oxidized compounds (Shiraiwa et al., 2014; Tong et

302 al., 2016). High aqueous oxidant levels may cause fragmentation of organic compounds,

303 resulting in an increased loss of carbon from the condensed phase (Daumit et al., 2016). The

Atmospheric Chemistry and Physics Discussions — Open Access — EGU

304 formed carbon- and oxygen-centred organic radicals are also expected to enhance chemical

305 aging by participating in particle-phase chemistry involving aldehydes, carbonyls, and

306 organic peroxides (Ziemann and Atkinson, 2012), although the exact role and impact of

307 formed organic radicals are still unclear and subject to further studies.

308   This study suggests that ROS can be generated in lung lining fluid upon inhalation

309 and respiratory deposition of atmospheric aerosol particles. Even though some fractions of

310 ROS may be scavenged by antioxidants contained in lung lining fluid, excess concentrations

311 of ROS including OH radicals, superoxide, and potentially also carbon- and oxygen centred

312 organic radicals may cause oxidative stress to lung cells and tissues (Winterbourn, 2008;

313 Pöschl and Shiraiwa, 2015; Tong et al., 2016). ROS play a central role in chemical

314 transformation of biomolecules such as proteins and lipids in lung fluid to form damage

315 associated molecular patterns (DAMPs), which can trigger immune reactions causing

316 inflammation through the toll-like receptor radical cycle (Lucas and Maes, 2013). Due to the

317 important implications to adverse aerosol health effects, further studies are warranted to

318 characterize and quantify EPFR and ROS contained in atmospheric aerosol particles in

319 various locations including highly polluted regions such as in East Asia and India.

320

321 **Appendix A. LC-MS analysis of organic mixtures**

322   Two solutions of mixtures of standard organic hydroperoxides and quinones were

323 analysed by liquid chromatography mass spectrometry (LC-MS). Solution (1) was the

324 mixture of 200 µL of p-benzoquinone solution at a concentration of 0.2 g L^{-1} (Reagent grade,

325 ≥98%, Sigma-Aldrich) in water (trace SELECT® Ultra, ACS reagent, for ultratrace analysis,

326 Sigma-Aldrich), 100 µL of Tert-Butyl hydroperoxide solution at a concentration of 8.9 g L^{-1}

327 (Luperox® TBH70X, 70 wt. % H$_2$O, Sigma-Aldrich) in water, 2.5 µL of Iron (II) sulfate

328 heptahydrate solution at 0.3 g L^{-1} (reagentPlus®, ≥99%, Sigma-Aldrich) in water and 1 mg of

329 5-tert-Butoxycarbonyl-5-methyl-1-pyrroline-N-oxide (BMPO, high purity, Enzo Life

330 Sciences GmbH). Solution (2) was the same as solution (1) but without Iron (II) sulfate

331 heptahydrate. These solutions were stirred with a vortex shaker (Heidolph Reax 1) for 5

332 minutes.

333   These solutions were analysed using a 1260 Infinity Bio-inert Quaternary LC system

334 with a quaternary pump (G5611A), a HiP sampler (G5667A) and an electrospray ionization

335 (ESI) source interfaced to a Q-TOF mass spectrometer (6540 UHD Accurate-Mass Q-TOF,

336 Agilent). All modules were controlled by the MassHunter software (B.06.01, Agilent). The

337 LC column was a Zorbax Extend-C18 Rapid resolution HT (2.1 x 50 mm, 1.8 µm) with a

Atmospheric
Chemistry
and Physics
Discussions

338 column temperature of 30 °C. The mobile phases were 3% (v/v) acetonitrile (HPLC Gradient

339 Grade, Fisher Chemical) in water with formic acid (0.1 % v/v, LC-MS Chromasolv, Sigma-

340 Aldrich) (Eluent A) and 3 % water in acetonitrile (Eluent B). The injection volume was 10

341 μL. The flow rate was 0.2 mL min^{-1} with a gradient program that starting with 3 % B for 3

342 min followed by a 36 minutes step that raised eluent B to 60 %. Further, Eluent B was

343 increased to 80 % at 40 minutes and returned to initial conditions within 0.1 minutes,

344 followed by column re-equilibration for 9.9 min before the next run.

345   The ESI-Q-TOF instrument was operated in the positive ionization mode (ESI+) with a

346 gas temperature of 325 °C, 20 psig nebulizer, 4000 V capillary voltage and 90 V fragmentor

347 voltage. During the full spectrum MS mode, no collision energy was used in order to collect

348 species as their molecular ions. During MS/MS analysis employed for the structure

349 determination, the fragmentation of protonated ions was conducted using the target MS/MS

350 mode with 20 V collision energy. Spectra were recorded over the mass range of m/z 50-1000.

351 Data analysis was performed using qualitative data analysis software (B.06.00, Agilent).

352 Blank solutions without BMPO were also prepared and analysed. Background signals were

353 subtracted from the MS spectrum.

354   Figure A2 shows LC-MS/MS mass spectra of the products formed from the reaction of

355 tert-butyl hydroperoxide, p-benzoquinone, BMPO in the presence of iron (solution 1). Very

356 similar results were obtained for solutions in the absence of iron (solution 2). BMPO adducts

357 with radicals ·OH, ·CH$_3$ and ·OCH$_3$ were identified by LC-MS/MS. As shown in Figure

358 A2(a.1), it was observed that ions at m/z 160.0596, 216.1221 and 238.1020 were majors ions

359 formed in the positive mode. These protonated ions represent the [BMPO+OH-C$_4$H$_8$+H]$^+$,

360 [BMPO+OH+H]$^+$ and [BMPO+OH+Na+H]$^+$ spin adducts, respectively. Figure A2 (a.2)

361 displays the mass spectrum in the MS/MS mode for the fragmentation of the ion m/z

362 216.1221. Results confirmed the loss of the t-butoxycarbonyl function (- C$_4$H$_8$), which is a

363 characteristic fragment of BMPO, to form the ion m/z 160.0585. The observed ion fragment

364 m/z 114.0544, can be formed by the loss of CH$_2$O$_2$, as shown in Fig. A2(a.3). In Fig. A2(b.1),

365 the spectrum showed the mass m/z 158.0804 and 214.1431 that can be attributed to the

366 [BMPO+CH$_3$-C$_4$H$_8$+H]$^+$ and [BMPO+CH$_3$+H]$^+$, respectively. The most abundant fragment

367 ion (m/z 158.0803) in the MS/MS mode confirmed the formation of BMPO+CH$_3$ adduct, as

368 shown in Fig. A2(b.2). The peak m/z 112.0752 can be formed by the loss of CH$_2$O$_2$ (Fig.

369 A2(b.3)). The spectrum in Fig. A2(c.1) shows major peaks at m/z 174.0752, 230.1378 and

370 252.1198, corresponding to [BMPO+OCH$_3$-C$_4$H$_8$+H]$^+$, [BMPO+OCH$_3$+H]$^+$ and

371 [BMPO+OCH$_3$+Na+H]$^+$, respectively. The formation of BMPO-OCH$_3$ was confirmed in

Atmospheric
Chemistry
and Physics
Discussions

372   MS/MS by the loss of the t-butoxycarbonyl functional group of BMPO to form the ion at m/z

373   174.0749 (panels (c.2) and (c.3)).

374   In addition, the radicals $C_6H_5O_2\cdot$ or $\cdot C_6H_5O_2$ and $C_6H_9O_2\cdot$ or $\cdot C_6H_9O_2$ were detected,

375   although it was not possible to determine whether the chemical structure represented carbon-

376   or oxygen-centred organic radicals using the applied method. Figure A3(a.1) shows the

377   formation of protonated ions $[BMPO+C_6H_5O_2+H]^+$ and $[BMPO+C_6H_5O_2+Na+H]^+$ with m/z

378   308.1475 and 330.1298, respectively. The fragmentation in the MS/MS mode confirms the

379   formation of $BMPO+C_6H_5O_2$ (m/z 252.0855) that correspond to the loss of the characteristic

380   t-butoxycarbonyl function as show in Fig. A3(a.2). The ion fragment observed m/z 128.0702,

381   can be formed by the loss of C_5O_4 (Figure A3(a.3)). Figure A3(b.1) shows the ion m/z

382   312.1789, which can be attributed to the $BMPO+C_6H_9O_2$ spin adduct. Figure A3(b.2)

383   suggests that the fragmentation of m/z 312.1789 to m/z 256.1166 by the loss of - C_4H_8 (Figure

384   A3(b.3)).

385

386   **Acknowledgements.**

389

390   **References.**

391   Abbas, K., Hardy, M., Poulhès, F., Karoui, H., Tordo, P., Ouari, O., and Peyrot, F.: Detection of
392   superoxide production in stimulated and unstimulated living cells using new cyclic nitrone spin traps,
393   Free Radical Biol. Med., 71, 281-290, 2014.

394   Badali, K. M., Zhou, S., Aljawhary, D., Antiñolo, M., Chen, W. J., Lok, A., Mungall, E., Wong, J. P.
395   S., Zhao, R., and Abbatt, J. P. D.: Formation of hydroxyl radicals from photolysis of secondary
396   organic aerosol material, Atmos. Chem. Phys., 15, 7831-7840, 2015.

397   Bahrle, C., Nick, T. U., Bennati, M., Jeschke, G., and Vogel, F.: High-Field Electron Paramagnetic
398   Resonance and Density Functional Theory Study of Stable Organic Radicals in Lignin: Influence of
399   the Extraction Process, Botanical Origin, and Protonation Reactions on the Radical g Tensor, The
400   journal of physical chemistry. A, 119, 6475-6482, 2015.

401   Berkemeier, T., Steimer, S., Krieger, U. K., Peter, T., Poschl, U., Ammann, M., and Shiraiwa, M.:
402   Ozone uptake on glassy, semi-solid and liquid organic matter and the role of reactive oxygen
403   intermediates in atmospheric aerosol chemistry, Phys. Chem. Chem. Phys., 18, 12662-12674, 2016.

404   Bond, T. C., Doherty, S. J., Fahey, D. W., Forster, P. M., Berntsen, T., DeAngelo, B. J., Flanner, M.
405   G., Ghan, S., Karcher, B., Koch, D., Kinne, S., Kondo, Y., Quinn, P. K., Sarofim, M. C., Schultz, M.
406   G., Schulz, M., Venkataraman, C., Zhang, H., Zhang, S., Bellouin, N., Guttikunda, S. K., Hopke, P.
407   K., Jacobson, M. Z., Kaiser, J. W., Klimont, Z., Lohmann, U., Schwarz, J. P., Shindell, D., Storelvmo,
408   T., Warren, S. G., and Zender, C. S.: Bounding the role of black carbon in the climate system: A
409   scientific assessment, J. Geophys. Res.-Atmos., 118, 5380-5552, 2013.

Atmospheric
Chemistry
and Physics
Discussions

410   Borrowman, C. K., Zhou, S., Burrow, T. E., and Abbatt, J. P.: Formation of environmentally
411   persistent free radicals from the heterogeneous reaction of ozone and polycyclic aromatic compounds,
412   Physical chemistry chemical physics : PCCP, 2015.

413   Charrier, J. G., McFall, A. S., Richards-Henderson, N. K., and Anastasio, C.: Hydrogen Peroxide
414   Formation in a Surrogate Lung Fluid by Transition Metals and Quinones Present in Particulate Matter,
415   Environ. Sci. Technol., 48, 7010-7017, 2014.

416   Chen, X., and Hopke, P. K.: A chamber study of secondary organic aerosol formation by limonene
417   ozonolysis, Indoor Air, 20, 320-328, 2010.

418   Chen, X., Hopke, P. K., and Carter, W. P.: Secondary organic aerosol from ozonolysis of biogenic
419   volatile organic compounds: chamber studies of particle and reactive oxygen species formation,
420   Environ Sci Technol, 45, 276-282, 2011.

421   Cho, A. K., Sioutas, C., Miguel, A. H., Kumagai, Y., Schmitz, D. A., Singh, M., Eiguren-Fernandez,
422   A., and Froines, J. R.: Redox activity of airborne particulate matter at different sites in the Los
423   Angeles Basin, Environ. Res., 99, 40-47, 2005.

424   Crounse, J. D., Nielsen, L. B., Jørgensen, S., Kjaergaard, H. G., and Wennberg, P. O.: Autoxidation of
425   organic compounds in the atmosphere, J. Phys. Chem. Lett., 4, 3513-3520, 2013.

426   Daumit, K. E., Carrasquillo, A. J., Sugrue, R. A., and Kroll, J. H.: Effects of Condensed-Phase
427   Oxidants on Secondary Organic Aerosol Formation, J. Phys. Chem. A, 120, 1386-1394, 2016.

428   Dellinger, B., Pryor, W. A., Cueto, R., Squadrito, G. L., Hegde, V., and Deutsch, W. A.: Role of free
429   radicals in the toxicity of airborne fine particulate matter, Chem. Res. Toxicol., 14, 1371-1377, 2001.

430   Dellinger, B., Loninicki, S., Khachatryan, L., Maskos, Z., Hall, R. W., Adounkpe, J., McFerrin, C.,
431   and Truong, H.: Formation and stabilization of persistent free radicals, Proc. Combust. Inst., 31, 521-
432   528, 2007.

433   Docherty, K. S., Wu, W., Lim, Y. B., and Ziemann, P. J.: Contributions of Organic Peroxides to
434   Secondary Aerosol Formed from Reactions of Monoterpenes with O3, Environmental Science &
435   Technology, 39, 4049-4059, 2005.

436   Dou, J., Lin, P., Kuang, B.-Y., and Yu, J. Z.: Reactive Oxygen Species Production Mediated by
437   Humic-like Substances in Atmospheric Aerosols: Enhancement Effects by Pyridine, Imidazole, and
438   Their Derivatives, Environ. Sci. Technol., 49, 6457-6465, 2015.

439   Ehn, M., Thornton, J. A., Kleist, E., Sipila, M., Junninen, H., Pullinen, I., Springer, M., Rubach, F.,
440   Tillmann, R., Lee, B., Lopez-Hilfiker, F., Andres, S., Acir, I.-H., Rissanen, M., Jokinen, T.,
441   Schobesberger, S., Kangasluoma, J., Kontkanen, J., Nieminen, T., Kurten, T., Nielsen, L. B.,
442   Jorgensen, S., Kjaergaard, H. G., Canagaratna, M., Dal Maso, M., Berndt, T., Petaja, T., Wahner, A.,
443   Kerminen, V.-M., Kulmala, M., Worsnop, D. R., Wildt, J., and Mentel, T. F.: A large source of low-
444   volatility secondary organic aerosol, Nature, 506, 476-479, 2014.

445   Enami, S., Sakamoto, Y., and Colussi, A. J.: Fenton chemistry at aqueous interfaces, Proc. Natl. Acad.
446   Sci. U.S.A., 111, 623-628, 2014.

447   Epstein, S. A., Blair, S. L., and Nizkorodov, S. A.: Direct photolysis of α-pinene ozonolysis secondary
448   organic aerosol: effect on particle mass and peroxide content, Environ. Sci. Technol., 48, 11251-
449   11258, 2014.

Atmospheric
Chemistry
and Physics
Discussions

450   Ervens, B.: Modeling the Processing of Aerosol and Trace Gases in Clouds and Fogs, Chem. Rev.,
451   115, 4157-4198, 2015.

452   Fang, T., Verma, V., Bates, J. T., Abrams, J., Klein, M., Strickland, M. J., Sarnat, S. E., Chang, H. H.,
453   Mulholland, J. A., Tolbert, P. E., Russell, A. G., and Weber, R. J.: Oxidative potential of ambient
454   water-soluble PM2.5 measured by Dithiothreitol (DTT) and Ascorbic Acid (AA) assays in the
455   southeastern United States: contrasts in sources and health associations, Atmos. Chem. Phys. Discuss.,
456   15, 30609-30644, 2015.

457   Fuller, S. J., Wragg, F. P. H., Nutter, J., and Kalberer, M.: Comparison of on-line and off-line
458   methods to quantify reactive oxygen species (ROS) in atmospheric aerosols, Atmos. Environ., 92, 97-
459   103, 2014.

460   Gehling, W., and Dellinger, B.: Environmentally Persistent Free Radicals and Their Lifetimes in
461   PM2.5, Environ. Sci. Technol., 47, 8172-8178, 2013.

462   Gehling, W., Khachatryan, L., and Dellinger, B.: Hydroxyl radical generation from environmentally
463   persistent free radicals (EPFRs) in PM2.5, Environ Sci Technol, 48, 4266-4272, 2014.

464   Gualtieri, M., Mantecca, P., Corvaja, V., Longhin, E., Perrone, M. G., Bolzacchini, E., and Camatini,
465   M.: Winter fine particulate matter from Milan induces morphological and functional alterations in
466   human pulmonary epithelial cells (A549), Toxicology letters, 188, 52-62, 2009.

467   Herrmann, H., Schaefer, T., Tilgner, A., Styler, S. A., Weller, C., Teich, M., and Otto, T.:
468   Tropospheric Aqueous-Phase Chemistry: Kinetics, Mechanisms, and Its Coupling to a Changing Gas
469   Phase, Chem. Rev., 115, 4259-4334, 2015.

470   Huang, C. H., Ren, F. R., Shan, G. Q., Qin, H., Mao, L., and Zhu, B. Z.: Molecular mechanism of
471   metal-independent decomposition of organic hydroperoxides by halogenated quinoid carcinogens and
472   the potential biological implications, Chem Res Toxicol, 28, 831-837, 2015.

473   Hung, H.-F., and Wang, C.-S.: Experimental determination of reactive oxygen species in Taipei
474   aerosols, Journal of Aerosol Science, 32, 1201-1211, 2001.

475   Jia, H., Nulaji, G., Gao, H., Wang, F., Zhu, Y., and Wang, C.: Formation and Stabilization of
476   Environmentally Persistent Free Radicals Induced by the Interaction of Anthracene with Fe(III)-
477   Modified Clays, Environ. Sci. Technol., 2016.

478   Jimenez, J. L., Canagaratna, M. R., Donahue, N. M., Prevot, A. S. H., Zhang, Q., Kroll, J. H.,
479   DeCarlo, P. F., Allan, J. D., Coe, H., Ng, N. L., Aiken, A. C., Docherty, K. S., Ulbrich, I. M.,
480   Grieshop, A. P., Robinson, A. L., Duplissy, J., Smith, J. D., Wilson, K. R., Lanz, V. A., Hueglin, C.,
481   Sun, Y. L., Tian, J., Laaksonen, A., Raatikainen, T., Rautiainen, J., Vaattovaara, P., Ehn, M., Kulmala,
482   M., Tomlinson, J. M., Collins, D. R., Cubison, M. J., Dunlea, E. J., Huffman, J. A., Onasch, T. B.,
483   Alfarra, M. R., Williams, P. I., Bower, K., Kondo, Y., Schneider, J., Drewnick, F., Borrmann, S.,
484   Weimer, S., Demerjian, K., Salcedo, D., Cottrell, L., Griffin, R., Takami, A., Miyoshi, T.,
485   Hatakeyama, S., Shimono, A., Sun, J. Y., Zhang, Y. M., Dzepina, K., Kimmel, J. R., Sueper, D.,
486   Jayne, J. T., Herndon, S. C., Trimborn, A. M., Williams, L. R., Wood, E. C., Middlebrook, A. M.,
487   Kolb, C. E., Baltensperger, U., and Worsnop, D. R.: Evolution of organic aerosols in the atmosphere,
488   Science, 326, 1525-1529, 2009.

489   Kampf, C. J., Liu, F., Reinmuth-Selzle, K., Berkemeier, T., Meusel, H., Shiraiwa, M., and Poschl, U.:
490   Protein Cross-Linking and Oligomerization through Dityrosine Formation upon Exposure to Ozone,
491   Environ Sci Technol, 49, 10859-10866, 2015.

492   Khachatryan, L., and Dellinger, B.: Environmentally Persistent Free Radicals (EPFRs)-2. Are Free
493   Hydroxyl Radicals Generated in Aqueous Solutions?, Environ. Sci. Technol., 45, 9232-9239, 2011.

494   Khachatryan, L., Vejerano, E., Lomnicki, S., and Dellinger, B.: Environmentally Persistent Free
495   Radicals (EPFRs). 1. Generation of Reactive Oxygen Species in Aqueous Solutions, Environ. Sci.
496   Technol., 45, 8559-8566, 2011.

497   Kumagai, Y., Arimoto, T., Shinyashiki, M., Shimojo, N., Nakai, Y., Yoshikawa, T., and Sagai, M.:
498   Generation of reactive oxygen species during interaction of diesel exhaust particle components with
499   NADPH-cytochrome P450 reductase and involvement of the bioactivation in the DNA damage, Free
500   Radical Biol. Med., 22, 479-487, 1997.

501   Lelieveld, J., Evans, J. S., Fnais, M., Giannadaki, D., and Pozzer, A.: The contribution of outdoor air
502   pollution sources to premature mortality on a global scale, Nature, 525, 367-371, 2015.

503   Lim, Y. B., Tan, Y., Perri, M. J., Seitzinger, S. P., and Turpin, B. J.: Aqueous chemistry and its role in
504   secondary organic aerosol (SOA) formation, Atmos. Chem. Phys., 10, 10521-10539, 2010.

505   Lin, P., and Yu, J. Z.: Generation of Reactive Oxygen Species Mediated by Humic-like Substances in
506   Atmospheric Aerosols, Environ. Sci. Technol., 45, 10362-10368, 2011.

507   Lucas, K., and Maes, M.: Role of the Toll Like Receptor (TLR) Radical Cycle in Chronic
508   Inflammation: Possible Treatments Targeting the TLR4 Pathway, Mol. Neurobiol., 48, 190-204, 2013.

509   McNeill, V. F., Woo, J. L., Kim, D. D., Schwier, A. N., Wannell, N. J., Sumner, A. J., and Barakat, J.
510   M.: Aqueous-phase secondary organic aerosol and organosulfate formation in atmospheric aerosols:
511   A modeling study, Environ. Sci. Technol., 46, 8075-8081, 2012.

512   McWhinney, R. D., Zhou, S., and Abbatt, J. P. D.: Naphthalene SOA: redox activity and
513   naphthoquinone gas–particle partitioning, Atmos. Chem. Phys., 13, 9731-9744, 2013.

514   Nel, A.: Air pollution-related illness: Effects of particles, Science, 308, 804-806, 2005.

515   Ouari, O., Hardy, M., Karoui, H., and Tordo, P.: Recent developments and applications of the coupled
516   EPR/Spin trapping technique (EPR/ST), in: Electron Paramagnetic Resonance: Volume 22, The Royal
517   Society of Chemistry, 1-40, 2011.

518   Pavlovic, J., and Hopke, P. K.: Detection of radical species formed by the ozonolysis of α-pinene,
519   Journal of Atmospheric Chemistry, 66, 137-155, 2011.

520   Pöhlker, C., Wiedemann, K. T., Sinha, B., Shiraiwa, M., Gunthe, S. S., Smith, M., Su, H., Artaxo, P.,
521   Chen, Q., Cheng, Y., Elbert, W., Gilles, M. K., Kilcoyne, A. L. D., Moffet, R. C., Weigand, M.,
522   Martin, S. T., Pöschl, U., and Andreae, M. O.: Biogenic potassium salt particles as seeds for
523   secondary organic aerosol in the Amazon, Science, 337, 1075-1078, 2012.

524   Pope, C. A., and Dockery, D. W.: Health effects of fine particulate air pollution: lines that connect, J.
525   Air Waste Manag. Assoc., 56, 709-742, 2006.

526   Pöschl, U., and Shiraiwa, M.: Multiphase Chemistry at the Atmosphere–Biosphere Interface
527   Influencing Climate and Public Health in the Anthropocene, Chem. Rev., 115, 4440–4475, 2015.

528   Reinmuth-Selzle, K., Ackaert, C., Kampf, C. J., Samonig, M., Shiraiwa, M., Kofler, S., Yang, H.,
529   Gadermaier, G., Brandstetter, H., Huber, C. G., Duschl, A., Oostingh, G. J., and Pöschl, U.: Nitration
530   of the birch pollen allergen Bet v 1.0101: Efficiency and site-selectivity of liquid and gaseous
531   nitrating agents, J. Proteome Res., 13, 1570−1577, 2014.

Atmospheric
Chemistry
and Physics
Discussions

Open Access

532   Saffari, A., Daher, N., Shafer, M. M., Schauer, J. J., and Sioutas, C.: Seasonal and spatial variation in
533   reactive oxygen species activity of quasi-ultrafine particles (PM0.25) in the Los Angeles metropolitan
534   area and its association with chemical composition, Atmos. Environ., 79, 566-575, 2013.

535   Saffari, A., Daher, N., Shafer, M. M., Schauer, J. J., and Sioutas, C.: Global perspective on the
536   oxidative potential of airborne particulate matter: a synthesis of research findings, Environ Sci
537   Technol, 48, 7576-7583, 2014.

538   Sanchez-Cruz, P., Santos, A., Diaz, S., and Alegria, A. E.: Metal-independent reduction of hydrogen
539   peroxide by semiquinones, Chem Res Toxicol, 27, 1380-1386, 2014.

540   Shaltout, A. A., Boman, J., Shehadeh, Z. F., Al-Malawi, D.-a. R., Hemeda, O. M., and Morsy, M. M.:
541   Spectroscopic investigation of PM2.5 collected at industrial, residential and traffic sites in Taif, Saudi
542   Arabia, Journal of Aerosol Science, 79, 97-108, 2015.

543   Shiraiwa, M., Sosedova, Y., Rouviere, A., Yang, H., Zhang, Y., Abbatt, J. P., Ammann, M., and
544   Poschl, U.: The role of long-lived reactive oxygen intermediates in the reaction of ozone with aerosol
545   particles, Nature chemistry, 3, 291-295, 2011.

546   Shiraiwa, M., Selzle, K., Yang, H., Sosedova, Y., Ammann, M., and Poschl, U.: Multiphase chemical
547   kinetics of the nitration of aerosolized protein by ozone and nitrogen dioxide, Environ Sci Technol, 46,
548   6672-6680, 2012.

549   Shiraiwa, M., Berkemeier, T., Schilling-Fahnestock, K. A., Seinfeld, J. H., and Pöschl, U.: Molecular
550   corridors and kinetic regimes in the multiphase chemical evolution of secondary organic aerosol,
551   Atmos. Chem. Phys., 14, 8323-8341, 2014.

552   Squadrito, G. L., Cueto, R., Dellinger, B., and Pryor, W. A.: Quinoid redox cycling as a mechanism
553   for sustained free radical generation by inhaled airborne particulate matter, Free Radical Biol. Med.,
554   31, 1132-1138, 2001.

555   Stoll, S., and Schweiger, A.: EasySpin, a comprehensive software package for spectral simulation and
556   analysis in EPR, Journal of magnetic resonance, 178, 42-55, 2006.

557   Strak, M., Janssen, N. A., Godri, K. J., Gosens, I., Mudway, I. S., Cassee, F. R., Lebret, E., Kelly, F.
558   J., Harrison, R. M., Brunekreef, B., Steenhof, M., and Hoek, G.: Respiratory health effects of airborne
559   particulate matter: the role of particle size, composition, and oxidative potential-the RAPTES project,
560   Environmental health perspectives, 120, 1183-1189, 2012.

561   Tong, H., Arangio, A. M., Lakey, P. S. J., Berkemeier, T., Liu, F., Kampf, C. J., Brune, W. H., Pöschl,
562   U., and Shiraiwa, M.: Hydroxyl radicals from secondary organic aerosol decomposition in water,
563   Atmos. Chem. Phys., 16, 1761-1771, 2016.

564   Truong, H., Lomnicki, S., and Dellinger, B.: Potential for Misidentification of Environmentally
565   Persistent Free Radicals as Molecular Pollutants in Particulate Matter, Environ. Sci. Technol., 44,
566   1933-1939, 2010.

567   Vejerano, E., Lomnicki, S., and Dellinger, B.: Formation and stabilization of combustion-generated
568   environmentally persistent free radicals on an Fe(III)2O3/silica surface, Environ Sci Technol, 45, 589-
569   594, 2011.

570   Venkatachari, P., Hopke, P. K., Grover, B. D., and Eatough, D. J.: Measurement of Particle-Bound
571   Reactive Oxygen Species in Rubidoux Aerosols, Journal of Atmospheric Chemistry, 50, 49-58, 2005.
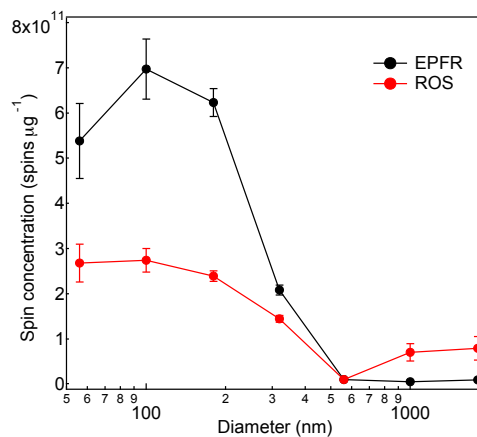
Atmospheric
Chemistry
and Physics
Discussions

572   Venkatachari, P., Hopke, P. K., Brune, W. H., Ren, X., Lesher, R., Mao, J., and Mitchell, M.:
573   Characterization of Wintertime Reactive Oxygen Species Concentrations in Flushing, New York,
574   Aerosol Science and Technology, 41, 97-111, 2007.

575   Verma, V., Fang, T., Xu, L., Peltier, R. E., Russell, A. G., Ng, N. L., and Weber, R. J.: Organic
576   aerosols associated with the generation of reactive oxygen species (ROS) by water-soluble PM2.5,
577   Environmental science & technology, 49, 4646-4656, 2015a.

578   Verma, V., Fang, T., Xu, L., Peltier, R. E., Russell, A. G., Ng, N. L., and Weber, R. J.: Organic
579   Aerosols Associated with the Generation of Reactive Oxygen Species (ROS) by Water-Soluble
580   PM2.5, Environ. Sci. Technol., 49, 4646-4656, 2015b.

581   Wang, D., Pakbin, P., Shafer, M. M., Antkiewicz, D., Schauer, J. J., and Sioutas, C.: Macrophage
582   reactive oxygen species activity of water-soluble and water-insoluble fractions of ambient coarse,
583   PM2.5 and ultrafine particulate matter (PM) in Los Angeles, Atmos. Environ., 77, 301-310, 2013.

584   Wang, Y., Kim, H., and Paulson, S. E.: Hydrogen peroxide generation from alpha- and beta-pinene
585   and toluene secondary organic aerosols, Atmos. Environ., 45, 3149-3156, 2011.

586   Wang, Y., Arellanes, C., and Paulson, S. E.: Hydrogen Peroxide Associated with Ambient Fine-Mode,
587   Diesel, and Biodiesel Aerosol Particles in Southern California, Aerosol Sci. Technol., 46, 394-402,
588   2012.

589   West, J. J., Cohen, A., Dentener, F., Brunekreef, B., Zhu, T., Armstrong, B., Bell, M. L., Brauer, M.,
590   Carmichael, G., Costa, D. L., Dockery, D. W., Kleeman, M., Krzyzanowski, M., Künzli, N., Liousse,
591   C., Lung, S.-C. C., Martin, R. V., Pöschl, U., Pope, C. A., Roberts, J. M., Russell, A. G., and
592   Wiedinmyer, C.: "What We Breathe Impacts Our Health: Improving Understanding of the Link
593   between Air Pollution and Health", Environ. Sci. Technol., 50, 4895-4904, 2016.

594   Winterbourn, C. C.: Reconciling the chemistry and biology of reactive oxygen species, Nature Chem.
595   Biol., 4, 278-286, 2008.

596   Zhao, H., Joseph, J., Zhang, H., Karoui, H., and Kalyanaraman, B.: Synthesis and biochemical
597   applications of a solid cyclic nitrone spin trap: a relatively superior trap for detecting superoxide
598   anions and glutathiyl radicals, Free Radical Biol. Med., 31, 599-606, 2001.

599   Zhu, B. Z., Kalyanaraman, B., and Jiang, G. B.: Molecular mechanism for metal-independent
600   production of hydroxyl radicals by hydrogen peroxide and halogenated quinones, Proc Natl Acad Sci
601   U S A, 104, 17575-17578, 2007a.

602   Zhu, B. Z., Zhao, H. T., Kalyanaraman, B., Liu, J., Shan, G. Q., Du, Y. G., and Frei, B.: Mechanism
603   of metal-independent decomposition of organic hydroperoxides and formation of alkoxyl radicals by
604   halogenated quinones, Proc Natl Acad Sci U S A, 104, 3698-3702, 2007b.

605   Zhu, B. Z., Shan, G. Q., Huang, C. H., Kalyanaraman, B., Mao, L., and Du, Y. G.: Metal-independent
606   decomposition of hydroperoxides by halogenated quinones: detection and identification of a quinone
607   ketoxy radical, Proc Natl Acad Sci U S A, 106, 11466-11471, 2009.

608   Ziemann, P. J., and Atkinson, R.: Kinetics, products, and mechanisms of secondary organic aerosol
609   formation, Chem. Soc. Rev., 41, 6582-6605, 2012.

610

611

Atmospheric
Chemistry
and Physics
Discussions

Open Access

EGU

612
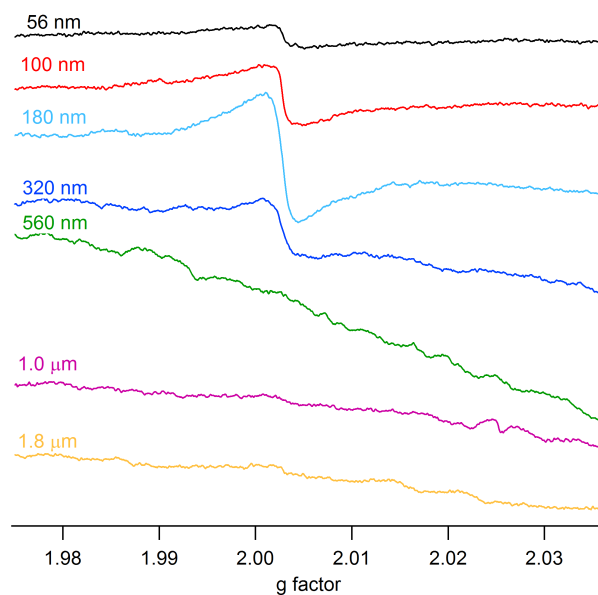
Figure 1: Electron paramagnetic resonance (EPR) spectra of atmospheric aerosol impactor

samples with lower cut-off diameters in the range of 56 nm to 1.8 micrometer collected in

Mainz, Germany during 26 - 27 June, 2015.

616

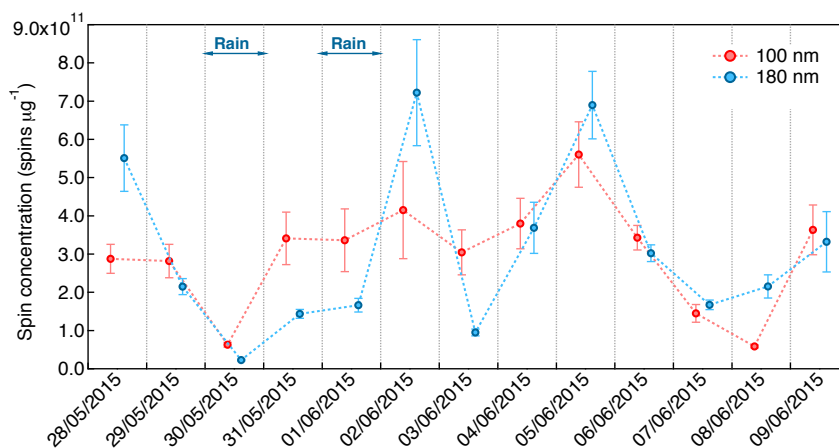

617

Figure 2: Concentrations (spins per microgram of particles) of environmentally persistent

free radicals (EPFR) and radical forms of reactive oxygen species (ROS) in atmospheric

aerosol samples plotted against particle diameter.

621

Atmospheric
Chemistry
and Physics
Discussions

Figure 3: Temporal evolution of concentrations of environmentally persistent free radicals (EPFR) contained in atmospheric aerosol samples with lower cutoff diameters of 100 nm (red) and 180 nm (blue), measured in Mainz, Germany during May – June 2015.
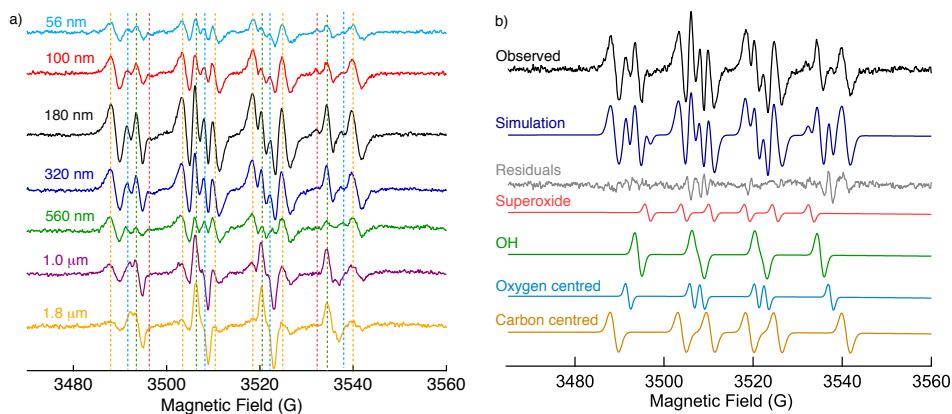
 Figure 4: a) Electron paramagnetic resonance (EPR) spectra of ambient aerosol impactor samples (Mainz, Germany, 26-27 June 2015) with lower cut-off diameters in the range of 56 nm to 1.8 μm extracted in water mixed with the spin-trapping agent BMPO. Dashed lines indicate the position of each peak for different types of trapped radicals of O_2^- (red), OH (green), carbon-centred (orange), and oxygen-centred organic radicals (light blue). b) Simulation of the EPR spectrum of the atmospheric aerosol impactor sample with particle diameters in the range of 180-320 nm (lower to upper cut-off) by deconvoluting into O_2^-, OH, O-centred and C-centred organic radicals (Blue = synthesis, grey = residual).
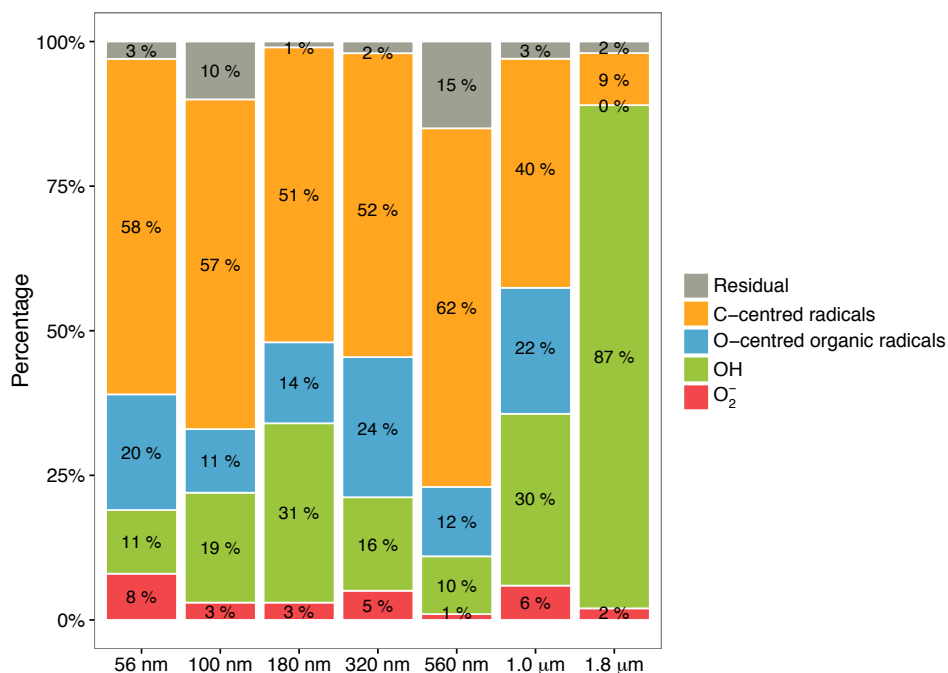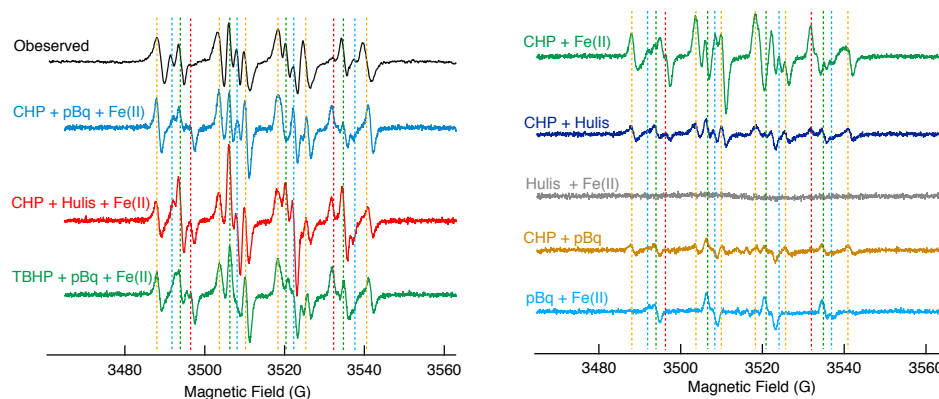
Figure 5: Relative amount of ROS in atmospheric aerosol impactor samples with lower cut-off diameters in the range of 50 nm -1.8 μm (Mainz, Germany, 26-27 June 2015): O_2^- (red), OH (green), carbon-centred (orange), oxygen-centred organic radicals (blue) and redisual (unidentified, grey).

Figure 6: Electron paramagnetic resonance (EPR) spectra of atmospheric aerosol impactor sample with particle diameters in the range of 180-320 nm (lower to upper cut-off) extracted with water and BMPO (black) and of aqueous substance mixtures with the following ingredients: cumene hydroperoxide (CHP), p-benzoquinone (pBq) and Fe(II) (light blue), t-butyl hydroperoxide (TBHP). The dashed vertical lines indicate the main peaks of BMPO adducts with O_2^- (red), OH (green), carbon- (light blown), and oxygen-centred organic radicals (light blue).

651

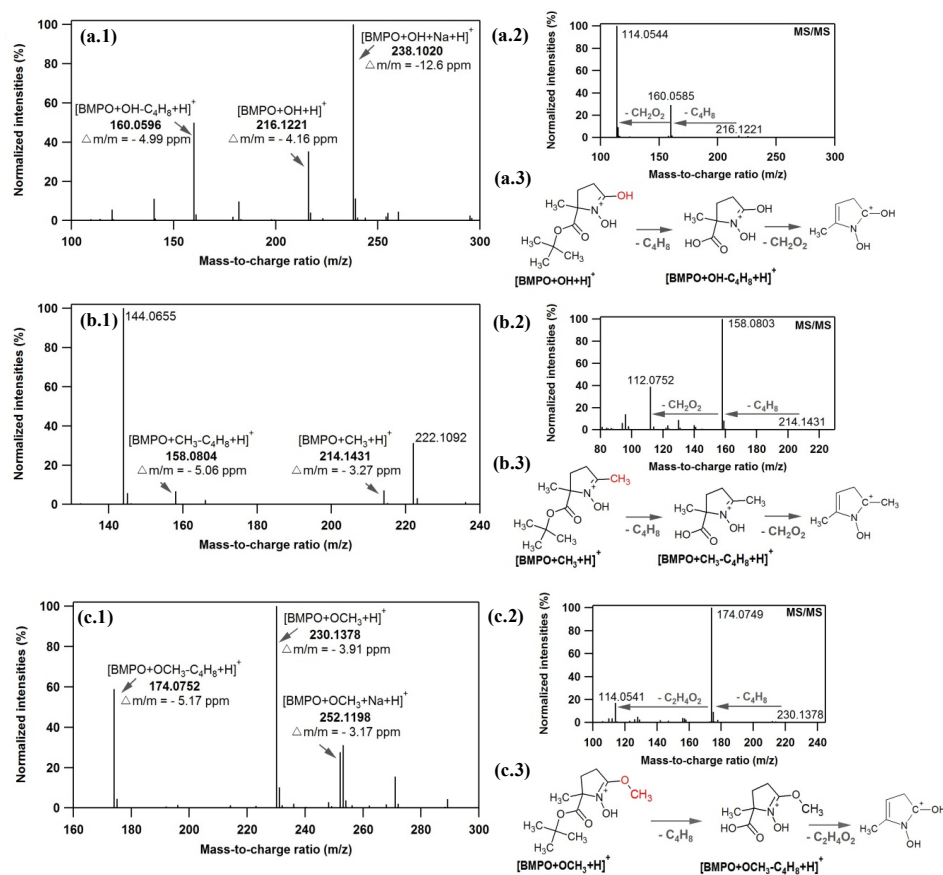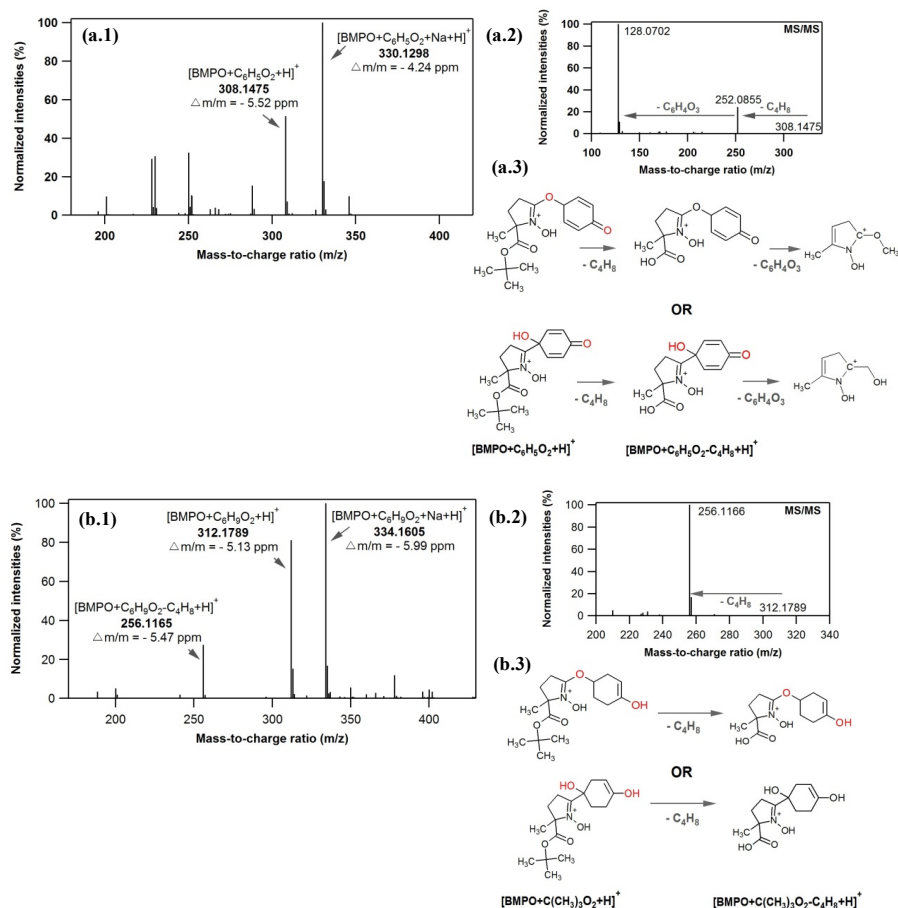652

653

654

655
656
657
658
659
660
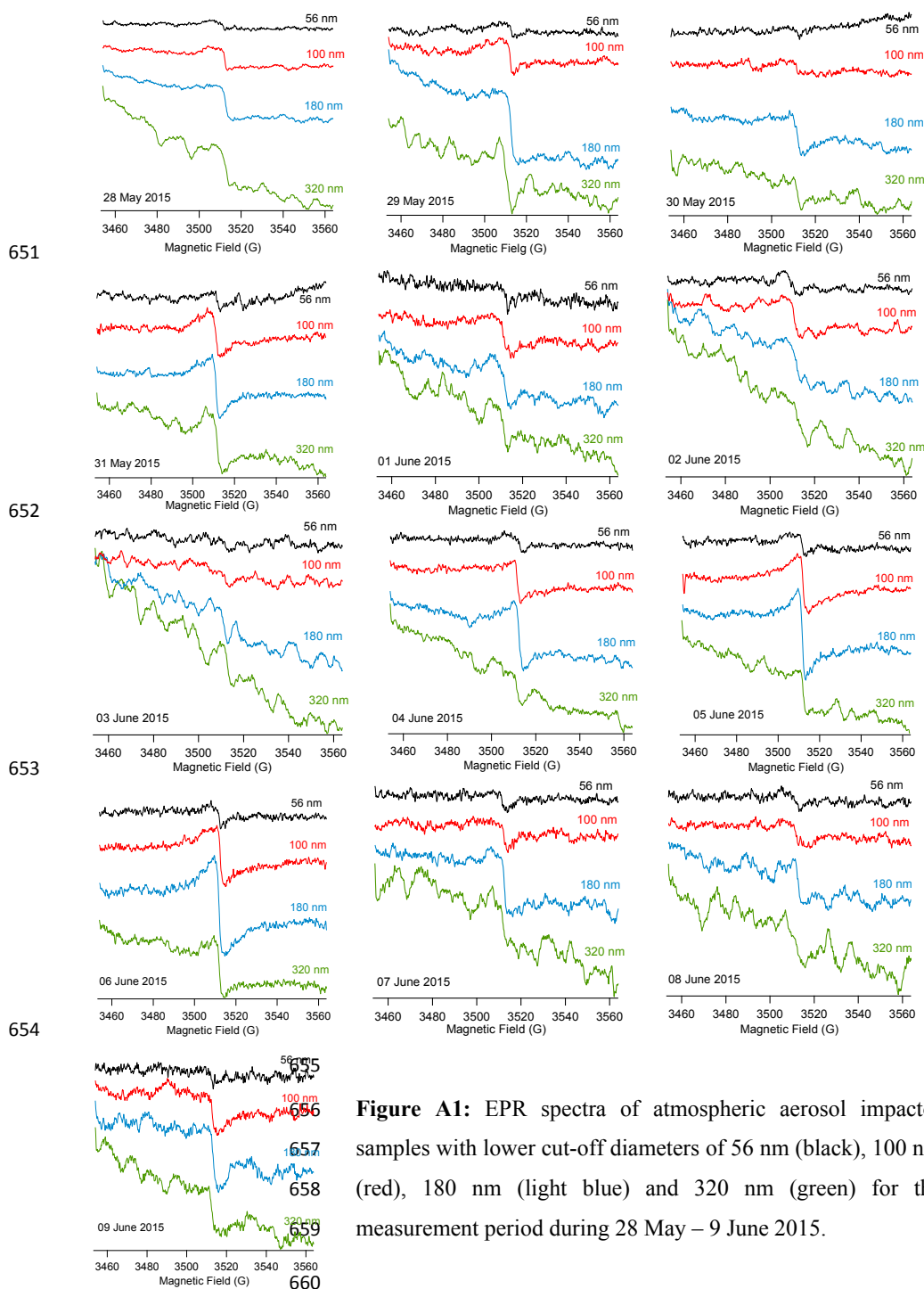
Figure A1: EPR spectra of atmospheric aerosol impactor samples with lower cut-off diameters of 56 nm (black), 100 nm (red), 180 nm (light blue) and 320 nm (green) for the measurement period during 28 May – 9 June 2015.

Figure A2: Mass spectra obtained with LC-MS/MS in the positive ionization mode from the mixture of tert-butyl hydroperoxide, p-benzoquinone and BMPO in the presence of iron (solution (1)). MS spectra of **(a.1)** BMPO+OH, **(b.1)** BMPO+CH_3 and **(c.1)** BMPO+OCH_3. MS/MS spectra of **(a.2)** BMPO+OH, **(b.2)** BMPO+CH_3, and **(c.2)** BMPO+OCH_3. Proposed fragmentation pathways of **(a.3)** BMPO+OH, **(b.3)** BMPO+CH_3 and **(c.3)** BMPO+OCH_3.

Atmospheric
Chemistry
and Physics
Discussions

Open Access

EGU

667

Figure A3: Mass spectra obtained with LC-MS/MS in the positive ionization mode for
solution (1). MS spectra of **(a.1)** BMPO+$C_6H_5O_2$ and **(b.1)** BMPO+$C_6H_9O_2$. MS/MS spectra
of **(a.2)** BMPO+$C_6H_5O_2$ and **(b.2)** BMPO+$C_6H_9O_2$. Proposed fragmentation pathway of **(a.3)**
BMPO+$C_6H_5O_2$ and **(b.3)** BMPO+$C_6H_9O_2$.